ACS APPLIED POLYMER MATERIALS

Article

Cite This: ACS Appl. Polym. Mater. 2019, 1, 2638−2648

pubs.acs.org/acsapm

Highly Uniform Activation of Carbon Fiber Reinforced Thermoplastics by Low-Temperature Plasma

Trey Oldham,[†] Kirby Simon,[‡] Daniel R. Ferriell,[∥] Marcus A. Belcher,[⊥] Alexander Rubin,[∥] and Elijah Thimsen*[,†,§]

[†]Department of Energy, Environmental and Chemical Engineering, [‡]Department of Mechanical Engineering and Materials Science, and [§]Institute of Materials Science and Engineering, Washington University, Saint Louis, Missouri 63130, United States

[∥]The Boeing Company, Saint Louis, Missouri 63134, United States

[⊥]The Boeing Company, Seattle, Washington 98124, United States

Supporting Information

ABSTRACT: Nonequilibrium plasma treatments of carbon fiber reinforced thermoplastic (CFRTP) composites can activate the robust, chemically inert material into a nonequilibrium state that can be used to fabricate bonded structural assemblies with high toughness. The nonequilibrium surface is unstable; thus, the development of nondestructive characterization techniques is of paramount importance to assess the material before use. Herein, a discovery is reported that plasma-activated CFRTP surfaces are characterized by a sharp, well-defined surface potential distribution, the width of which is correlated to the fracture toughness of bonded assemblies. The activated surface has a maximum lifetime on the order of days to weeks and is hypothesized to be composed of metastable radical-ion complexes. The hypothesis is consistent with several independent pieces of evidence, including Kelvin probe force microscopy, contact angle measurements, magnetic force microscopy, and radical probe experiments.

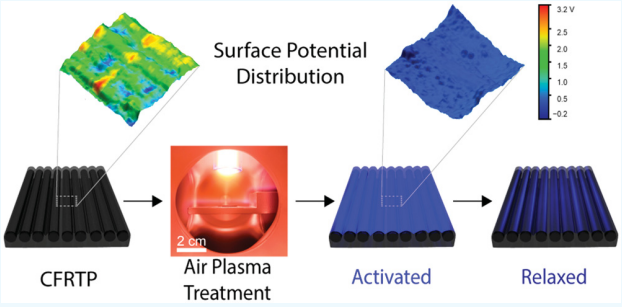

KEYWORDS: *plasma treatment, carbon fiber, polymer-matrix composites (PMCs), surface modification, oxygen plasma activation, scanning probe microscopy*

INTRODUCTION

There is a need to improve fuel efficiency in transportation applications without sacrificing performance, which motivates the development of lightweight structural materials. Carbon fiber reinforced polymer composites are a leading class of lightweight structural materials.[1] Compared to traditional structural materials, carbon fiber reinforced polymer composites offer the advantage of tailorable strength and stiffness, corrosion resistance, and lower assembly costs. Additionally, adhesive joining of composites enables advantages in composite manufacturing and design when compared to use of mechanical fasteners. However, inadequate surface preparation of bonded assemblies can result in adhesion failure, and subsequent structural failure, at low loads. Qualified bonded processes must be repeatable and reliable.[2] If the failure mode and value of a joint are not consistent, then it is challenging to design a bonded structure. Therefore, materials, processes, and instruments to reliably produce consistent joints are critical for large acreage bonded structures.

Poly(aryl ether ketone)s (PAEKs) are a family of semicrystalline thermoplastics with a molecular backbone comprised of alternately arranged ether and ketone groups, interconnected by para-substituted benzene rings. PAEKs are characterized by their high-temperature thermal stability, chemical resistance, and high mechanical strength. Engineered PAEK thermoplastics, such as poly(ether ketone ketone) (PEKK), have recently attracted attention as the matrix material. Thermoplastics offer a number of advantages over traditionally used thermosets. Compared to thermosets, thermoplastics have lower processing cost, improved toughness, and are more easily recycled. While thermosets must be stored in cold, dry environments to minimize any reactions that degrade the material and lower its shelf life, thermoplastics are relatively inert and can be stored at ambient conditions for nearly indefinite periods of time. Additionally, the relatively low moisture uptake of thermoplastics makes them robust under hot and wet conditions, in comparison to thermosets, which can experience significant deterioration of mechanical properties in damp environments. From a mechanical perspective, thermoplastics typically have high fracture toughness values, which is a measure of durability and strength. This high fracture toughness is a result of the semicrystalline

Received: June 17, 2019
Accepted: September 3, 2019
Published: September 3, 2019

DOI: 10.1021/acsapm.9b00532
ACS Appl. Polym. Mater. 2019, 1, 2638−2648

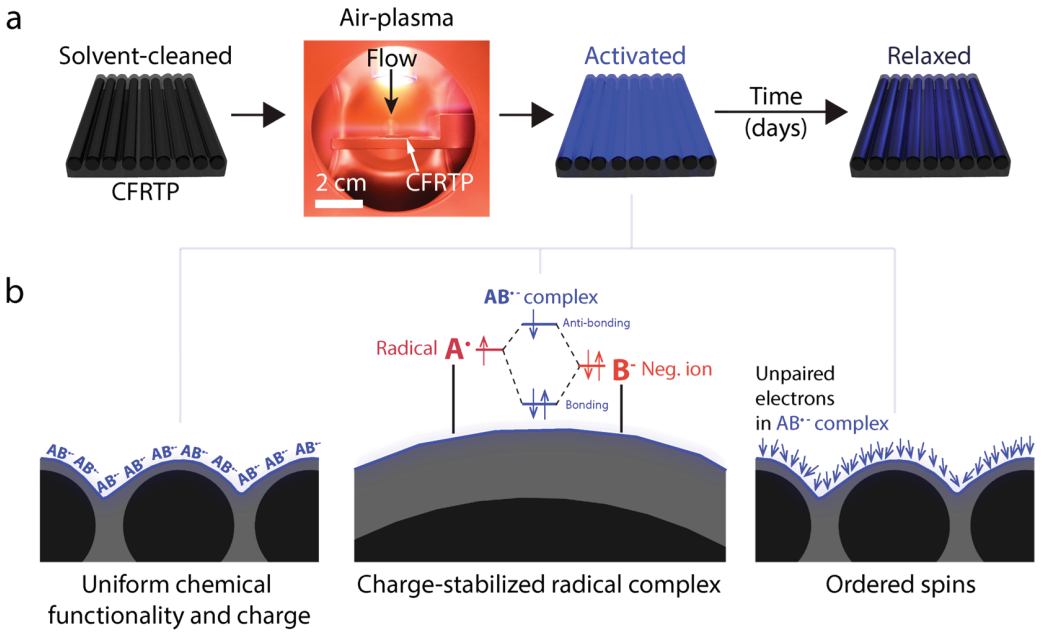

Figure 1. Overview of (a) sample preparation and (b) key results. (a) The surface of a CFRTP composite is activated by a low-temperature air plasma into a highly nonequilibrium state, which subsequently relaxes over several days. (b) The plasma-activated surface is highly uniform and composed of radical species ($A^{\bullet}$, e.g., $ROO^{\bullet}$) that are stabilized by colocalized negative ions (B^{-}, e.g., RO^{-}). The unpaired electrons in the $AB^{\bullet-}$ complex are ordered on the surface such that a net magnetic moment is produced. It should be noted that although the scheme depicts one radical per charge, several radicals could be stabilizing one charge, or vice versa.

structure of the material. The crystalline regions increase the tensile strength while the amorphous regions allow for more effective absorbing of impact energy. The superior chemical resistance of thermoplastics improves durability in the wide variety of environments that an aircraft or automobile may encounter. However, this chemical inertness also raises a challenge: robustly bonding different components into a structural assembly.

It has been known for decades that if the surfaces of polymer components are treated with a low-temperature oxygen-containing plasma before bonding, then adhesion in bonded assemblies can be significantly improved.[3−7] Despite the ubiquitous usage of plasma processing of polymers in applications including lithography,[8−10] microfluidics,[11−13] and biomedical,[14−19] the effect is not well understood from a molecular perspective. Oxygen-containing plasmas can etch carbonaceous materials[20−24] and can also remove contaminants from surfaces.[25] Thus, the effect has often been described as plasma cleaning. In other words, plasma treatment exposes a clean surface composed of the material. The cleaning concept implies that the surface ought to be stable if the material were stored in an environment free of chemical and physical contamination, but that implication is contradicted by experimental observations.[26−28]

Another hypothesis is that the material surface is activated by the low-temperature plasma into a highly reactive state characterized by a much higher chemical potential compared to the equilibrium surface. Low-temperature plasma is a highly nonequilibrium substance and a potent source of energetic species that bombard surfaces exposed to it; for example, electrons and ions with sufficient energy to dissociate chemical bonds (on the order of 1 eV),[5] chemical radicals,[29] and high-energy photons.[30] Differing from the cleaning concept, an activated surface would be intrinsically unstable and expected to decay at some system-dependent rate. Therefore, measurement of the activation state becomes critical to ensure that the surface is adequately prepared for subsequent processing. By use of the activation concept, the challenge becomes characterizing the highly nonequilibrium surface without destroying its chemical functionality. That challenge has not been previously overcome, and a solution is essential if one hopes to fundamentally understand the nature of the nonequilibrium surface and use it for some application.

In this work, a discovery is reported that can be used as the basis for new nondestructive characterization of the activation state of CFRTP composites treated by low-temperature air plasma. The key observation is that plasma treatment produces a well-defined surface characterized by a very sharp distribution of electron electrochemical potential, with a mean potential that is significantly greater than untreated control specimens. The phenomenon was revealed by Kelvin probe force microscopy (KPFM) surface potential mapping. The width of the surface potential distribution changed with intensity of plasma treatment and time elapsed after plasma exposure. For different plasma treatment intensities and time after treatment, the standard deviation of the surface potential distribution could be correlated to fracture toughness determined by double cantilever beam (DCB) testing of bonded assemblies of CFRTP components. Narrower surface potential distributions before bonding were correlated to higher fracture toughness of bonded assemblies. Characterization of the plasma-activated CFRTP surface was found to be consistent with the hypothesis that the key chemical functional groups are charges that colocalize with and stabilize adjacent radicals, forming radical-ion complexes as shown in Figure 1b.[31,32] Interestingly, the unpaired electrons in the colocalized radical-ion complexes appear to be ordered, producing a net magnetic moment on the surface in a particular orientation (Figure 1b).

DOI: 10.1021/acsapm.9b00532
ACS Appl. Polym. Mater. 2019, 1, 2638−2648

EXPERIMENTAL SECTION

Materials. The preparation of the composite materials is described below. Platinum−iridium (Pt−Ir) coated conductive atomic force microscopy (AFM) probes (SCM-PIT-V2) and cobalt−chromium (Co−Cr) coated magnetic AFM probes (MESP-V2) were purchased from Bruker Nano (Camarillo, CA). The radical probe Pyrogallol-sulfonephthalein (pyrogallol red, PGR) was purchased from MilliporeSigma (St. Louis, MO).

Plasma Treatments of CFRTP Composite Surfaces. Three types of CRFTP samples were prepared: control, low plasma dose, and high plasma dose. All samples consisted of HexTow AS4D carbon fibers (Hexcel, Stamford, CT) embedded in a thermoplastic PEKK matrix, which were cut from one large panel (i.e., they were all initially part of the same panel) with a thickness of 0.8 mm. Samples for material characterization were nominally 12 × 12 mm^2 while panels to be bonded were approximately 152 × 381 mm^2. All samples for DCB testing were solvent cleaned by wiping with methyl ethyl ketone. The control samples were not processed any further. The plasma was generated at atmospheric pressure using air as the process gas in an Openair FG5001 plasma generator (Plasmatreat) with a 16 mm diameter jet equipped with an an 17° rotary nozzle. Treatment was performed by moving the plasma head over the sample at a rate of 6.4 or 13 mm s^{-1} for high and low dose plasma, respectively. The plasma source parameters were held constant but treatment time was varied. Plasma treatment times of 1.2 and 2.5 s were used for low and high dose, respectively. Atmospheric pressure plasma treatment and bonding procedures were performed in a clean room environment with actively monitored relative humidity (RH), which at all times was in the range from 40 to 50%. Characterization of samples was performed as a function of time after plasma treatment, ranging from 0 to 7 days.

CFRTP samples used to test for functional groups, thermal properties, and lap shear testing were treated with a laboratory-built plasma unit that also consisted of a 16 mm diameter plasma jet generated using a radio-frequency power supply (AG 0613, T&C Power Conversion) at an applied power set point of 50 W and frequency of 13.56 MHz. The power was coupled to the powered electrode through an impedance matching network (AIT-600 RF Auto Tuner, T&C Power Conversion). The powered electrode was an aluminum ring wrapped around the outside of a 19 mm outer diameter fused silica tube. The plasma flowed through the tube and impinged upon the sample. An image of the custom plasma system during operation is presented in Figure 1a. The plasma was generated in a gas mixture of 70.6% Ar, 7.3% O_2, and 22.2% N_2 at a total mass flow rate of 248 sccm (standard cubic centimeters per minute) and total pressure of 1.20 mbar. The samples were allowed to settle in the vacuum for 5 min prior to plasma exposure. Plasma exposure was performed for a duration of 4 min. The approximate background gas temperature of the plasma was 102.3 °C. Experiments focused on comparing the commercial plasma unit to the custom unit found that they were very similar in their effect on the CFRTP composite surfaces. Unless otherwise stated, samples were stored in an environment with a strictly controlled RH of 48% prior to characterization. Ambient temperature was controlled in all of the laboratories to be in the range from 18 to 24 °C. For both the low- and atmospheric-pressure plasma systems, characterization was conducted on duplicate samples to determine statistical variations between subsequent surface treatments.

Double Cantilever Beam Testing. Double cantilever beam (DCB) testing was used to evaluate bonded assemblies. Fabricated samples complied with ASTM D5528-13 requirements.[33] Unidirectional CFRTP tape was preconsolidated into DCB adherends. The faying surfaces of each 152 mm × 381 mm DCB parent panel were prepared by plasma treatment. After treatment, two CFRTP samples were bonded, with a crack starter on one side, by using a 177 °C curing structural epoxy adhesive cured in an autoclave. After curing, the panels were machined into individual coupons ∼12.7 × 381 mm^2 in size, with a 125 mm crack starter present. The fracture toughness of the bonded samples was determined by prying the samples apart under controlled conditions and using the average of three measurements, in compliance with ASTM D5528-13.[33] After mechanical testing, coupons were opened fully to evaluate failure mode. Each data point is the average of three different measurements at the same combination of the two independent variables (plasma dose and time after treatment). The reported values are the average of those three measurements performed on nominally identical samples, and the error bars are the standard deviations.

Lap Shear Testing. Lap shear testing was used to evaluate bonded assemblies prepared with the laboratory-built plasma unit. Single lap-shear joints were fabricated using unidirectional CFRTP samples that were cut into to 25.4 mm × 25.4 mm coupons prior to bonding and cleaned using the aforementioned procedure. For the plasma-treated samples, each surface used for bonding was prepared using the laboratory-built plasma unit. Adhesively bonded joints were assembled using a two-component structural adhesive (Loctite Hysol EA 9394 AERO Epoxy) and applied to the adherend surfaces such that the epoxy covered a 25.4 mm × 12.7 mm area. A 0.15 mm thick scrim fabric was cut to the same 25.4 mm × 12.7 mm size and overlaid onto the epoxy-coated area of one coupon. The two coupons were bonded such that the bond-line thickness was approximately equal to the scrim thickness. A constant pressure of 1360 mbar was applied to the bonded assemblies while they were being cured in a furnace maintained at a temperature of 75 °C for 3.5 h. Following the cure cycle, the bonded assemblies were removed from the furnace and kept at the same applied pressure under ambient conditions for 24 h prior to tensile testing. Tensile testing was performed using an electromechanical universal testing machine (Instron 5583) at room temperature. The bonded assemblies were pulled apart by using a 150 kN load cell with a constant loading rate of 1.25 mm/min. The load at failure was taken as the maximum applied load recorded prior to assembly failure. The reported load at failures are averages of repeated measurements on nominally identical samples for a given treatment condition. The error bars are the standard deviation of the load at failure.

Surface Potential Measurements. The distribution of values for the electrochemical potential of electrons on the CFRTP surface was measured by using Kelvin probe force microscopy (KPFM). KPFM is a nondestructive characterization method that relies on relatively long-range electrostatic effects. In principle, KPFM can be performed without touching the sample. However, for the experiments used to compare surface potential and fracture toughness, contact was made in PeakForce Tapping mode to acquire topography. PeakForce KPFM (PF-KPFM) measurements were conducted using a Dimension Icon atomic force microscope (AFM; Bruker) in air under ambient conditions. Fresh Pt−Ir coated conductive probes were used for each sample in the PF-KPFM measurements. A scanning area of 10 μm × 10 μm, a tip velocity of 11.9 μm s^{-1}, and a lift height of 95 nm were used for all sample measurements. For each sample, topography and surface potential maps were acquired for several locations at random. At least three nominally identical samples were characterized for each combination of independent variables.

Experiments also focused on correlating surface potential to lap shear strength using a laboratory-built Kelvin probe (KP). Unlike PF-KPFM, the KP allowed for macroscopic measurements to be made without making physical contact with the samples. Others have discussed the operating principles of KPs at length,[34] and thus only the specifics of our experiments are presented here. The surface potential was measured using an oscillating stainless steel tip, 3 mm in diameter, at a frequency of 110 Hz, positioned ∼300 μm above the CFRTP sample. CFRTP samples were divided into a 3 × 3 grid such that nine different spatial locations were characterized for each sample, allowing for the determination of an average and standard deviation. For each spatial location on the sample, after the appropriate probe-to-sample distance was established, a series of 21 backing voltages from −0.5 to 1.5 V were scanned. For each of those backing voltages, a data acquisition device (DAQ) recorded from a current preamplifier (Keithley 6482, Tektronix) the current waveform in the measurement circuit. The current waveform was processed using a Fourier transform to determine the amplitude at the tip

DOI: 10.1021/acsapm.9b00532
ACS Appl. Polym. Mater. 2019, 1, 2638−2648

oscillation frequency of 110 Hz. At each spatial location, three scans were performed and the values were averaged to reduce random error. After performing signal processing, the current amplitude at the tip oscillation frequency was plotted as a function of applied backing voltage, and linear fits were used to determine the null voltage, or surface potential, of each spatial location.

It is important to note that surface potential measurements, both PF-KPFM and KP, are susceptible to changes in RH due to the buildup of charge (hygroelectricity) and surface potential shielding.[35,36] All experiments were performed in a controlled laboratory environment that had a measured RH in the range of 48−51% at all times.

Magnetic Force Microscopy and Quantitative Nanomechanical Mapping. The magnetic moment of organic radicals can be mapped on a surface by magnetic force microscopy (MFM).[37,38] The phase shift produced by the force between tip and sample in an MFM experiment includes contributions from both electrostatic and magnetic interactions. If the sample exhibits a net magnetic moment in a particular direction, then electrostatic contributions to the phase shift can be eliminated by mapping the same region of the sample with equal but oppositely magnetized probes that are otherwise identical, a method termed controlled magnetism MFM (Supporting Information Note 1).[39,40] The phase shift map of the repulsed probe was subtracted from the phase shift map of the attracted probe to eliminate electrostatic contributions to the force gradient.

MFM and PeakForce quantitative nanomechanical mapping (PFQNM) were performed using a Dimension Icon AFM (Bruker) in air under ambient conditions. The RH was in the range of 48−51% for all reported experiments. Fresh Co−Cr coated magnetic probes were used for each sample in the MFM and PFQNM measurements. Co−Cr probes were magnetized with a neodymium magnet (>11.5 kOe) prior to each measurement. A scanning area of 15 μm × 15 μm, a tip velocity of 23.9 μm s^{-1}, and a lift height of 95 nm were used for all samples. The deflection sensitivity and spring constant for PFQNM probes were calibrated using a commercially available sapphire standard (SAPPHIRE-12M, Bruker) prior to each measurement. Additional details for scanning probe experiments can be found in the Supporting Information.

X-ray Photoelectron Spectroscopy (XPS). The elemental surface composition of plasma and untreated samples was examined by using XPS on a PHI 5000 VersaProbe II (Physical Electronics) operated at a base pressure of 8.6 × 10^{-7} Pa using a monochromatic Al Kα line (1486.6 eV) with a power of 25 W, a spot size of 100.0 μm, and a takeoff angle of 45° between the analyzer and the sample surface. Survey spectra were acquired using a pass energy of 117.40 eV and a step size of 1.0 eV. The C 1s and O 1s high-resolution spectra were acquired using a pass energy of 23.5 eV and a step size of 0.05 eV.

Differential Scanning Calorimetry (DSC). The effects of plasma treatment on the thermal properties of the PEKK matrix were determined by differential scanning calorimetry (DSC, Model DSC2500, TA Instruments). Plasma-treated and untreated samples (5−6 mg) were sealed in hermetic aluminum pans and heated at a rate of 20 °C min^{-1} under a nitrogen atmosphere from 40 to 380 °C to remove the thermal history of the polymers. The crystallization temperatures were determined by maintaining samples at 380 °C for 5 min before cooling to 220 °C at a rate of 20 °C min^{-1}. The melting point of the polymers were determined by maintaining samples at 220 °C for 5 min prior to being heated to 380 °C at a rate of 20 °C min^{-1}. Samples were subsequently quench cooled to 50 °C and maintained for 5 min. The glass transition temperature for each sample was found by an additional heating to 200 °C at a rate of 20 °C.

Bipolar Ion Exposure. Select samples were plasma treated and then exposed to a gaseous bipolar ion source to neutralize surface charges introduced by plasma treatment. An AC static eliminator bar (Model 400T Ion Edge, TAKK Industries) was used as the bipolar ion source, delivering gaseous positive and negative ion output to eliminate static charges on the CFRTP surface. Plasma-treated CFRTP composite samples were placed 2.0 cm away from the static eliminator bar and treated for a duration of 48 h under ambient conditions. An experiment was performed to measure ion concentration at the sample surface during bipolar ion exposure. Two parallel tungsten wires were positioned 2.0 cm away from the source. The wires were 0.36 mm in diameter and 15 mm in length and separated by a distance of 0.3 mm. A voltage was applied between the two wires, and the resulting current flow was used to determine the conductance of the air containing the bipolar ions. The conductive air was modeled using a paraxial cylindrical geometry for the electrodes to determine conductivity. The ion concentration was calculated under the assumption that there were an equal number of positive and negative charges. The ion mobilities for positive and negative ions were taken from the literature[41] to be 1.15 × 10^{-4} and 1.43 × 10^{-4} m^2 V^{-1} s^{-1}, respectively. The resulting ion concentration was determined to be 2.8 × 10^7 cm^{-3}, which is similar to ion concentrations reported for other bipolar sources.[41] Plasma-treated samples not exposed to bipolar ions were stored under the same ambient conditions for the same duration so direct comparisons could be made with minimal influence of aging effects.

Radical Probing Experiments. Pyrogallolsulfonephthalein (pyrogallol red, PGR) reacts strongly with reactive oxygen species (ROS). The chemical structure of PGR contains three hydroxyl groups in an aromatic conjugated chromophore system. In aqueous solution, PGR shows a strong maximum absorbance band at 540 nm. As PGR is consumed, that absorbance band decreases proportionally to concentration. Fresh 40 μM PGR solutions in 75 mM phosphate buffer solution (PBS, pH 7.4) were prepared prior to each experiment. Plasma-treated and control samples were stored in ambient conditions for the same duration as the bipolar ion exposure. The bipolar ion sample was exposed continuously for 48 h after plasma treatment. All samples were placed in 10 mL of PGR solution made from the same stock solution. The samples, in addition to a 10 mL pure PGR solution used for comparison, were allowed to react at 40 °C for an hour before ultraviolet−visible (UV−vis) absorption spectroscopy. UV−vis absorption spectroscopy was performed by transferring 0.1 mL aliquots of each solution into a cuvette and diluting with 1 mL of PBS. The decrease in peak absorbance for the PGR band at ∼540 nm was used to monitor the relative amount of ROS present in a sample. Decreased absorbance corresponds to increased areal density of radicals on the sample surface. UV−vis absorbance spectra were measured on a Cary 50 Bio spectrophotometer (Varian). Spectra were acquired over the wavelength range of 300−800 nm using a scan rate of 300 nm min^{-1}. Pure PBS was used as the blank for baseline subtraction.

RESULTS AND DISCUSSION

Exposing CFRTP composite to low-temperature air plasma has three effects: (1) it produces a narrower surface potential distribution compared to the untreated control, (2) it shifts the mean surface potential to much more negative values, indicating an increase in average electron energy on the surface, and (3) it increases the fracture toughness and lap shear strength of bonded assemblies. The surface potential can be related to the energy of electrons on the surface, more specifically the electrochemical potential of electrons before contact:

$$-eV_{sp} = \bar{\mu}_e^s - \bar{\mu}_e^p \quad (1)$$

where e is the elementary charge, V_{sp} is the measured surface potential, $\bar{\mu}_e^s$ is the position-dependent electrochemical potential of electrons on the sample surface before contact, and $\bar{\mu}_e^p$ is the electrochemical potential of electrons in the probe before contact. The electrochemical potential of a species is the sum of the chemical potential and the electrostatic potential energy:[42]

$$\bar{\mu}_e^i = \mu_e^i + z_e e\psi_i \quad (2)$$

DOI: 10.1021/acsapm.9b00532
ACS Appl. Polym. Mater. 2019, 1, 2638−2648

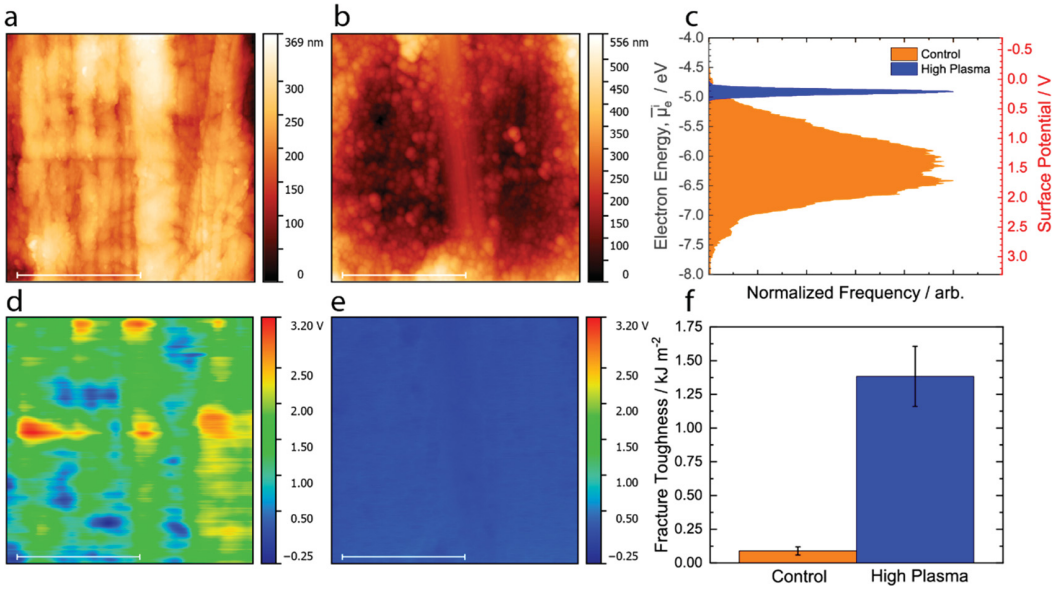

Figure 2. Plasma activation of CFRTP composite. Topographical and surface potential maps of (a, d) solvent-cleaned control and (b, e) high-dose plasma-treated samples. The scale bars are 5 μm wide. (c) Histograms of electron energy $\overline{\mu}_e^i$ (and surface potential) for samples (d) and (e). The histograms have been normalized such that their maximum value is 1. (f) Fracture toughness, determined from double cantilever beam experiments, of assemblies made of components pretreated in different ways: solvent-cleaned control (orange) and high-dose plasma (blue).

where $\overline{\mu}_e^i$ is the electrochemical potential of an electron in phase i, μ_e^i is the chemical potential of an electron in phase i, z_e is the charge number (−1 for an electron), and ψ_i is the electrostatic potential of phase i. Herein, electron energy will refer to the electrochemical potential of an electron. The expectation is that if the material only has a few types of chemical functional groups and uniform areal density of surface charge, then the distribution of surface potential values will be narrow. Conversely, if the surface has many types of chemical functional groups and/or an uneven areal density of surface charge, then the surface potential distribution will be broad. In other words, a narrow surface potential distribution indicates both chemical and surface charge uniformity while a broad surface potential distribution indicates a large number of different chemical groups, uneven surface charge, or both. Note that a positive surface potential value is not necessarily indicative of a positively charged sample surface before contact. Rather, a more positive surface potential indicates that the work function of the sample, which is influenced by both surface chemistry and electrostatic surface charge (eq 2), is less than the work function of the Pt−Ir tip. A more detailed explanation of KPFM theory can be found in Supporting Information Note 2.

CFRTP samples treated with high plasma dose resulted in significantly more narrow surface potential distributions and higher fracture toughness values compared to untreated controls. Examples of topography and surface potential maps are presented in Figure 2 for untreated control (2a, 2d) and high-dose plasma (2b, 2e) specimens. Histograms of the electron energy (and surface potential) on the surface of the control and high dose plasma specimens are presented in Figure 2c, wherein the distributions have been normalized such that the maximum value is 1, and the electron energy value was determined via eq 1 with a calibrated work function for the PF-KPFM probe (Supporting Information Note 2). As shown in Figure 2c, electron energy (and surface potential) distribution for the untreated control is broad while the plasma-treated sample is narrow. Moreover, the mean value shifted to a higher electron energy, or more negative surface potential, after plasma treatment. The trends for these two representative examples were also observed in the statistical data set, the results of which are summarized in Table 1. Specifically, the mean surface potential value for control samples was 1.43 V, which shifted to more negative values of 0.34 and 0.15 V, respectively, for the low- and high-dose plasma treatments (i.e., higher electron energy). Likewise, surface potential distributions became increasingly narrow with more intense plasma treatments relative to untreated controls. At the 0 day time point, the standard deviation decreased from 0.539 V for the untreated control, to 0.076 V for low-dose plasma, to 0.041 V for high-dose plasma. Note that the surface potential measurements were made immediately after plasma treatment.

Table 1. Summary of Surface Potential (SP) and Fracture Toughness (G_{IP}) Experiments[a]

treatment	time (days)	⟨SP⟩ (V)	σ_{SP} (V)	G_{IP} (kJ m^{-2})
none	0	1.43	0.539	0.05 ± 0.02
low	0	0.34	0.076	0.68 ± 0.07
low	1	0.08	0.062	0.88 ± 0.36
low	3	0.08	0.069	0.33 ± 0.05
low	7	0.22	0.089	0.41 ± 0.14
high	0	0.15	0.041	1.31 ± 0.14
high	1	0.11	0.024	1.17 ± 0.22
high	3	0.10	0.030	1.00 ± 0.09
high	7	0.10	0.040	0.77 ± 0.15

[a]The mean (⟨SP⟩) and averaged standard deviation (σ_{SP}) of the surface potential values were determined by at least two measurements per sample and at least three samples for each pair of independent variables. Time corresponds to time after treatment. Each value for G_{IP} was determined from at least three experiments at nominally the same pair of independent variables. The error bar on G_{IP} is the standard deviation.

DOI: 10.1021/acsapm.9b00532
ACS Appl. Polym. Mater. 2019, 1, 2638−2648

Interestingly, the standard deviation of surface potential distribution for the high-dose plasma was close to the value of k_BT/e = 0.026 V at room temperature, which indicates a well-defined surface (Table 1). These results are consistent with plasma exposure creating a surface with a uniform areal density of surface charge and uniform chemical functionality. The negative shift in the mean value of the surface potential (or increase in electron energy) distribution suggests that plasma treatment has caused the surface to become negatively charged with respect to the control (Supporting Information Note 2). Interestingly, the fracture toughness of assemblies composed of coupons treated with a high-dose plasma before bonding was ~28 times higher than untreated controls (Figure 2f). For DCB assemblies made with a high plasma dose, failure occurred either in the adhesive (cohesion failure) or in the composite itself (interlaminar failure). In other words, for high plasma dose, the bond between adhesive and CFRTP was stronger than the cohesive strength of the composite itself (Supporting Information Note 3). It may be concluded that plasma treatment produces a well-defined CFRTP surface with few types of chemical functional groups and uniform negative charge and that activated surface results in very high fracture toughness for bonded assemblies compared to untreated CFRTP.

The standard deviation of the surface potential distribution, σ_{SP}, is expected to be inversely correlated to the fraction of the surface covered in activated functional groups. Therefore, an inverse relationship is expected between the standard deviation of surface potential distribution before bonding and the fracture toughness of bonded assemblies. Coupons were treated by using either a low plasma dose or high plasma dose, and then 0−7 days were allowed to elapse before bonding into an assembly for subsequent DCB testing. Fracture toughness of the bonded assemblies as a function of time after treatment is plotted in Figure 3a. In general, fracture toughness decreased with time after treatment, presumably resulting from relaxation of the nonequilibrium surface. The reciprocal of the standard deviation of the surface potential distribution is plotted as a function of time after treatment in Figure 3b. The different plasma treatments could be clearly distinguished from one another (Figure 3b), and thus σ_{SP}^{-1} appears to be a promising way of describing the activation state of the CFRTP surface. The high and low plasma doses appear to pass through a maximum as a function of time after treatment. These maxima are believed to be caused by an initial imbalance in the areal density of radicals and electrostatic charges, and a faster decay rate for the species that is present in excess, which is also expected to be unevenly distributed. By plotting the fracture toughness at a given time as a function of σ_{SP}^{-1} at that same time point, one can observe that higher values of σ_{SP}^{-1} correlated to higher fracture toughness values (Figure 3c). Thus, measurement of the surface potential distribution appears to be an attractive, nondestructive method to assess the activation state of a CFRTP composite before bonding it into a structural assembly. While the surface potential distribution appears promising as a fundamental descriptor of the activated surface that can be used to judge if a surface has been adequately prepared, the specific means of measurement presented above (i.e., scanning probe microscopy) is likely impractical in manufacturing settings. That point raises a question: can the macroscopic surface potential distribution measured before

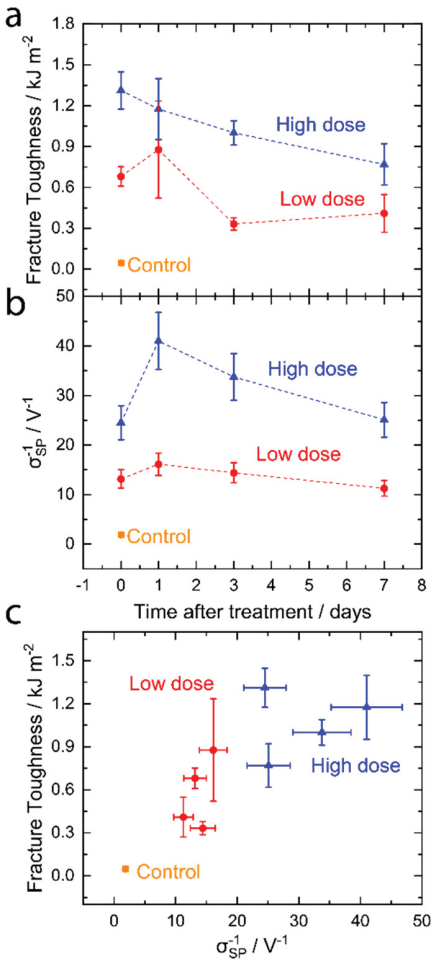

Figure 3. Correlation between fracture toughness and nanoscopic σ_{SP}. (a) Fracture toughness as a function of time after different plasma treatments. (b) Reciprocal of σ_{SP} as a function of time after different plasma treatments. (c) Correlation between σ_{SP}^{-1} and fracture toughness. The data in (c) are the same as (a) and (b).

bonding by a blunt probe with size on the order of 1 mm also be correlated to the strength of bonded assemblies?

By use of a blunt probe, the laboratory-built KP detected a narrowing of the surface potential distribution on a macroscopic length scale and that was correlated to the load at failure of bonded assemblies characterized by single-lap shear testing. Macroscopically, when compared to untreated control samples, a smaller σ_{SP} value was measured for plasma-activated samples up to 5 days after treatment. To develop a correlation between standard deviation of the macroscopic surface potential distribution and strength of adhesively bonded assemblies, single-lap shear testing was performed on nominally identical samples. In other words, sets of samples were plasma treated under identical conditions and then allowed to age before adhesive bonding into assemblies: 1, 2, 3, or 5 days after activation. For a given aging period, the surface potential distribution was measured using 10 mm × 10 mm samples that had undergone identical plasma treatments as those used for lap shear testing. As seen with the DCB testing, plasma treatment of CFRTP composites prior to adhesive bonding increased the resulting assembly strength, indicated by an increased load at failure compared to control assemblies. For plasma-treated samples, failure primarily occurred in the

DOI: 10.1021/acsapm.9b00532
ACS Appl. Polym. Mater. 2019, 1, 2638−2648

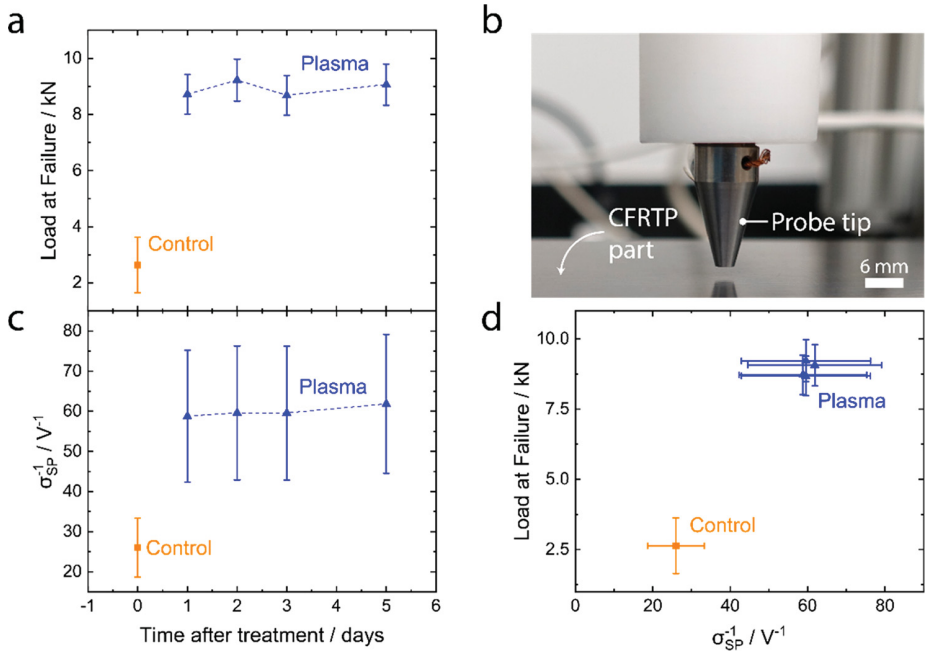

Figure 4. Correlation between load at failure and macroscopic σ_{SP}. (a) Load at failure as a function of time after plasma treatment. (b) Image of KP system used for macroscopic surface potential measurements. (c) Reciprocal of macroscopic σ_{SP} as a function of time after plasma treatments using laboratory-built unit. (d) Correlation between macroscopic σ_{SP}^{-1} and load at failure. The data in (d) are the same as (a) and (c).

Table 2. Summary of DSC Experiments[a]

treatment	T_m (°C)	T_c (°C)	T_g (°C)	X_c (%)
none	340.35 ± 0.02	278.16 ± 0.09	161.15 ± 0.19	34.0 ± 2.5
plasma	340.38 ± 0.34	278.30 ± 0.24	161.75 ± 0.87	33.3 ± 4.4

[a]The mean values for the melting (T_m), crystallization (T_c), and glass transition (T_g) temperatures and crystallinity (X_c) were determined by using the DSC thermograms of three nominally identical samples for plasma and control samples. The error bars are the standard deviations.

composite material itself (interlaminar failure). For control samples, all bonded assemblies experienced adhesion failure. Images of the fracture surfaces, as well as a summary of the failure types for each treatment type, can be found in Supporting Information Note 4. Figures 4a and 4c respectively show the load at failure, as measured by lap shear testing, and the σ_{SP}^{-1} values, as measured by the macroscopic laboratory-built KP, for different aging times. Note that for the plasma-treated samples, at all of the measured time points, the cohesive strength of the composite was less than the adhesive strength of the bond. Thus, the load at failure did not change due to the fact that the cohesive strength, an intrinsic property of the composite, did not change with time. Plotting load at failure as a function of σ_{SP}^{-1} (Figure 4d) produces a similar result to what was found with the nanoscopic PF-KPFM measurements and DCB testing of assemblies (*vide supra*), indicating there was a positive correlation between large σ_{SP}^{-1} values and increased load at failure of adhesively bonded assemblies. Interestingly, the width of both nanoscopic and macroscopic surface potential distributions appear to correlate to the strength of adhesively bonded assemblies. That observation supports the surface potential distribution as a descriptor that can be used to characterize the activation state of CFRTP composites prior to bonding without destroying the chemical functionality of the material. Furthermore, the macroscopic laboratory-built KP is amenable to practical application as a quality control instrument in bonded composite assembly manufacturing.

Plasma treatment clearly changed the surface properties of the CFRTP (*vide infra*); however, bulk properties of the polymer matrix such as melting temperature, glass transition temperature, and crystallinity remain unaltered. For example, XPS revealed a significant change in the chemical speciation of the CFRTP surface after plasma treatment, specifically a higher oxygen content (Supporting Information Note 5). The bulk properties were investigated by DSC to discern if plasma treatment had changed the structure of the polymer. For example, chemical alteration of the polymer would result in different interactions between chains, and a change in bulk properties such as glass transition temperature, melting point, or crystallinity. DSC was performed to elucidate the influence that plasma treatment had on the thermal properties of the PEKK matrix. As summarized in Table 2, no appreciable changes in melting temperature, crystallization temperature, or glass transition temperature were observed after plasma treatment. The crystallinity of the samples was calculated by using the enthalpies of fusion obtained from the thermograms (Supporting Information Note 6). The average crystallinity of control and plasma-treated samples were determined to be 34.0% and 33.3%, respectively, which are the same value considering the precision of the experiment (Table 2). Our evidence demonstrates that exposing CFRTP to low-temperature air plasma results in changes to chemical functionality of the surface; however, bulk properties remain unaltered. Because plasma treatment changed surface chemistry but not

DOI: 10.1021/acsapm.9b00532
ACS Appl. Polym. Mater. 2019, 1, 2638−2648

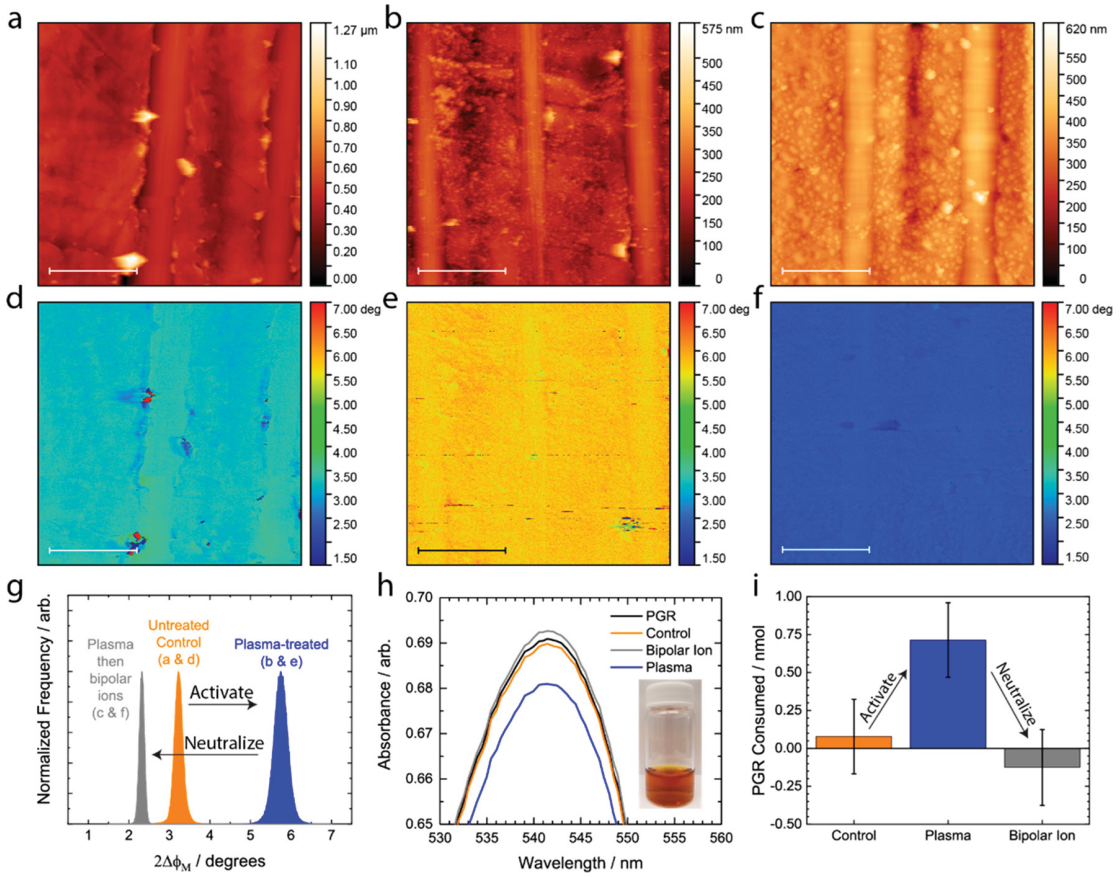

Figure 5. Evidence for charge-stabilized radicals. Topographical and phase-shift difference maps of CFRTP samples prepared using different treatments: (a, d) untreated control, (b, e) plasma treated, and (c, f) plasma treated followed by exposure to bipolar ions. The scale bars are 5 μm. Phase shift difference maps were generated by subtracting the MFM map acquired using an M+ probe from the MFM map acquired using an M− probe (Supporting Information Note 1). (g) Histograms of the phase shift difference maps in (d−f). (h) Visible absorbance spectra of solutions composed of pyrogallol red (PGR) dissolved in phosphate buffer solutions after exposure to samples prepared using the same procedures as (a−f). The curve labeled PGR corresponds to the stock solution. The plasma-treated sample exhibited the lowest PGR absorbance, indicating it had consumed the most PGR and therefore had the highest radical density. (i) The amount of PGR consumed by the sample surface as determined by Beer−Lambert law. The error bars in (i) were determined by root-sum-of-squares combination of the intrinsic spectrometer noise with the standard deviation of repeat measurements performed on nominally identical samples.

bulk properties, the surface chemistry of activated CRFTP composite was further investigated.

The hypothesis is that the plasma-activated polymer composite surface is composed of organic radical species that are stabilized by organic anions. Additionally, these radicals are hypothesized to be associated with oxygen. It is well-documented that organic radicals ($R^{\bullet}$) generated by low-temperature plasma treatment of polymer surfaces react with gas phase O_2 to form peroxyl radicals ($ROO^{\bullet}$).[43] Furthermore, low-temperature plasmas containing oxygen are a well-known source of oxygen radicals,[44] such as monatomic oxygen,[29,45] and thus it is reasonable to expect oxygen-bearing radicals on the surface. In the laboratory-built plasma system used here, a correlation between monatomic oxygen triplet biradical density in the plasma, measured by optical emission spectroscopy, and σ_{SP}^{-1}, measured from surfaces of plasma-treated CFRTP samples, was experimentally observed (Supporting Information Note 7). The activated surface of the CFRTP composite was unstable and decayed on a time scale of several days after plasma exposure (Figure 3). A lifetime of days is somewhat long for a highly reactive species such as a peroxyl radical. One explanation is that the radicals are stabilized by colocalized electrostatic surface charge, which has been used to account for the behavior of mechanically generated radicals and charges on other polymers, including polydimethylsiloxane.[33,34] Floating surfaces in contact with low-temperature plasmas are expected to adopt a negative charge to balance the flux of electrons and positive ions to maintain overall charge neutrality in the plasma.[46] Thus, a negative surface charge for the CFRTP sample is expected, and KPFM data support that hypothesis wherein the mean surface potential after plasma treatment was clearly shifted to a value more negative than the untreated control (Figure 2c and Table 1). The high density of negative charge on the CFRTP surface is expected to stabilize radical species by the recently proposed charge stabilization effect, whereby formation of frontier molecular orbitals between colocalized organic radicals and surface ions results in a complex that has lower energy compared to the radical and ion in isolation (Supporting Information Note 8 and Figure 1b).

A number of pieces of evidence indicate the presence of charge-stabilized radical species on the surface after plasma exposure and are consistent with the presence of $ROO^{\bullet}$ species colocalized and stabilized by negative charge. XPS revealed a dramatic increase in the amount of oxygen on the CFRTP

DOI: 10.1021/acsapm.9b00532
ACS Appl. Polym. Mater. 2019, 1, 2638−2648

surface after plasma exposure and that oxygen was bonded to carbon (Supporting Information Note 5). Contact angle measurements revealed that the plasma-activated surface behaved as an electron donor, which is consistent with the expected behavior of a colocalized anion-radical complex (Supporting Information Note 8). The unpaired electrons associated with anion-radical complexes would also have a magnetic moment. Force−distance curves measured by using oppositely but equally magnetized probes in an atomic force microscope (AFM) revealed that the surface became magnetized after plasma exposure with a spin ordering that produced a net magnetic moment opposite to the direction of the macroscopic sample surface normal (Supporting Information Note 1). The sample surface magnetization due to plasma exposure can be more clearly characterized by controlled magnetism MFM.

Controlled magnetism MFM phase shift difference maps, in which the magnetic contribution to the force gradient between sample and probe has been isolated, are presented in Figure 5e for a representative plasma-treated sample. Phase shift difference maps are included for an untreated control (Figure 5d) as well as a plasma-treated sample that was subsequently exposed to bipolar ions to neutralize surface charge (Figure 5f). Histograms of the phase shift difference maps for all three samples are presented in Figure 5g. The average magnetic force between sample and tip increased with plasma treatment compared to the control and then decreased when the surface charge was neutralized by exposure to air containing bipolar ions with a concentration of 2.8×10^7 cm^{-3} (Figure 5g). In other words, plasma treatment uniformly increased the density of magnetic spins on the surface, and then electrostatic neutralization by exposure to bipolar ions decreased it (Figure 5g).

Furthermore, experiments conducted using a radical probe known to be consumed by reactive oxygen species (ROS, e.g., the peroxyl radical[47]) revealed a similar trend (Supporting Information Note 9). The amount of PGR consumed by the sample surface was approximately zero for the control, increased to a value of 0.71 nmol after plasma treatment and then decreased to approximately zero after exposure to bipolar ions (Figure 5h,i). To rule out changes in PGR adsorption due to changes in oxygen content of the surface, the bond speciation of each sample was examined by XPS (Supporting Information Note 5). When compared to the amount of PGR consumed (Figure 5i) and the effect on surface spin density (Figure 5g), it was found that bipolar ion exposure had a negligible effect on both the amount of oxygen on the plasma treated surface and its speciation (Supporting Information Note 5). Oxygen present in the C−O bonds is presumably initially a radical after plasma exposure, but during neutralization it becomes destabilized by bipolar ions, reacting to form a functional group which does not interact with PGR (e.g., an alcohol). The results support the hypothesis that oxygen-containing radicals produced by plasma treatment are stabilized by colocalized negative electrostatic charges.

CONCLUSIONS

In summary, a discovery has been reported herein that the width of the surface potential distribution of plasma-treated CFRTP components is correlated to the fracture toughness of bonded assemblies made from those components. Macroscopic measurements made using a laboratory-built Kelvin probe revealed behavior similar to nanoscopic measurements made using a commercial scanning probe microscope, emphasizing the practicality of the discovery. Surface potential distribution measurements could be used for quality control in processes that involve plasma activation of thermoplastics prior to bonding. Scanning probe measurements of CFRTP samples revealed a sharp peak in the surface potential distribution after plasma treatment, indicative of a surface that has a uniform areal density of electrostatic charge and few types of chemical functional groups. Conversely, the untreated samples showed a wider surface potential distribution, suggestive that the surface was nonuniform in electrostatic charge and chemical functionality. Thermal analysis of the polymeric matrix indicated that plasma treatments resulted in negligible changes to the bulk properties of the thermoplastic. The evidence suggests that the well-defined plasma-activated CFRTP composite surface is composed of organic oxygen-containing radicals colocalized with and stabilized by negative electrostatic charges.

ASSOCIATED CONTENT

Supporting Information

The Supporting Information is available free of charge on the ACS Publications website at DOI: 10.1021/acsapm.9b00532.

Discussion of controlled magnetism MFM, force vs distance curves, surface potential measurements and work functions, example failure surfaces, XPS spectra, DSC thermograms and crystallinity calculations, effect of water composition in the air plasma, qualitative explanation of charge-stabilized radicals, and UV−vis absorption spectra and radical areal density calculations (PDF)

AUTHOR INFORMATION

Corresponding Author

*E-mail: elijah.thimsen@wustl.edu.

ORCID

Trey Oldham: 0000-0002-4058-1490

Elijah Thimsen: 0000-0002-7619-0926

Notes

The authors declare no competing financial interest.

ACKNOWLEDGMENTS

The authors acknowledge financial support from the National Science Foundation (NSF) under grant agreement PHY-1702334, Washington University in Saint Louis Institute of Materials Science and Engineering and Nano Research Facility for the use of instruments and staff assistance. The authors thank J. D. Fortner for the use of the UV−vis absorbance spectrophotometer.

REFERENCES

(1) Wu, G. Effects of Carbon Fiber Treatment on Interfacial Properties of Advanced Thermoplastic Composites. *Polym. J.* **1997**, *29*, 705−707.

(2) AC 20-107B - Composite Aircraft Structure − Document Information; https://www.faa.gov/regulations_policies/advisory_circulars/index.cfm/go/document.information/documentID/99693.

(3) Kinloch, A. J.; Kodokian, G. K. A.; Watts, J. F. The Adhesion of Thermoplastic Fibre Composites. *Philos. Trans. R Soc. London, A* **1992**, *338*, 83−112.

(4) Awaja, F.; Gilbert, M.; Kelly, G.; Fox, B.; Pigram, P. J. Adhesion of Polymers. *Prog. Polym. Sci.* **2009**, *34*, 948−968.

DOI: 10.1021/acsapm.9b00532
ACS Appl. Polym. Mater. 2019, 1, 2638−2648

(5) Vesel, A.; Mozetic, M. New Developments in Surface Functionalization of Polymers Using Controlled Plasma Treatments. *J. Phys. D: Appl. Phys.* **2017**, *50*, 293001.
(6) Cui, L.; Ranade, A. N.; Matos, M. A.; Dubois, G.; Dauskardt, R. H. Improved Adhesion of Dense Silica Coatings on Polymers by Atmospheric Plasma Pretreatment. *ACS Appl. Mater. Interfaces* **2013**, *5*, 8495−8504.
(7) Juárez-Moreno, J. A.; Ávila-Ortega, A.; Oliva, A. I.; Avilés, F.; Cauich-Rodríguez, J. V. Effect of Wettability and Surface Roughness on the Adhesion Properties of Collagen on PDMS Films Treated by Capacitively Coupled Oxygen Plasma. *Appl. Surf. Sci.* **2015**, *349*, 763−773.
(8) Korczagin, I.; Golze, S.; Hempenius, M. A.; Vancso, G. J. Surface Micropatterning and Lithography with Poly(Ferrocenylmethylphenylsilane). *Chem. Mater.* **2003**, *15*, 3663−3668.
(9) Campos, L. M.; Truong, T. T.; Shim, D. E.; Dimitriou, M. D.; Shir, D.; Meinel, I.; Gerbec, J. A.; Hahn, H. T.; Rogers, J. A.; Hawker, C. J. Applications of Photocurable PMMS Thiol−Ene Stamps in Soft Lithography. *Chem. Mater.* **2009**, *21*, 5319−5326.
(10) Kaya, S.; Rajan, P.; Dasari, H.; Ingram, D. C.; Jadwisienczak, W.; Rahman, F. A Systematic Study of Plasma Activation of Silicon Surfaces for Self Assembly. *ACS Appl. Mater. Interfaces* **2015**, *7*, 25024−25031.
(11) Khademhosseini, A.; Suh, K. Y.; Jon, S.; Eng, G.; Yeh, J.; Chen, G.-J.; Langer, R. A Soft Lithographic Approach To Fabricate Patterned Microfluidic Channels. *Anal. Chem.* **2004**, *76*, 3675−3681.
(12) Xu, J.; Gleason, K. K. Conformal, Amine-Functionalized Thin Films by Initiated Chemical Vapor Deposition (ICVD) for Hydrolytically Stable Microfluidic Devices. *Chem. Mater.* **2010**, *22*, 1732−1738.
(13) Cao, H. H.; Nakatsuka, N.; Liao, W.-S.; Serino, A. C.; Cheunkar, S.; Yang, H.; Weiss, P. S.; Andrews, A. M. Advancing Biocapture Substrates via Chemical Lift-Off Lithography. *Chem. Mater.* **2017**, *29*, 6829−6839.
(14) Bazaka, K.; Jacob, M. V.; Crawford, R. J.; Ivanova, E. P. Plasma-Assisted Surface Modification of Organic Biopolymers to Prevent Bacterial Attachment. *Acta Biomater.* **2011**, *7*, 2015−2028.
(15) Slepicka, P.; Slepickova Kasalkova, N.; Stranska, E.; Bacakova, L.; Svorcik, V. Surface Characterization of Plasma Treated Polymers for Applications as Biocompatible Carriers. *eXPRESS Polym. Lett.* **2013**, *7*, 535−545.
(16) Yamazaki, K.; Yakushiji, T.; Sakai, K. Nanoscale Analysis of Hydrophilicity−Hydrophobicity Distribution on Inner Surfaces of Wet Dialysis Membranes by Atomic Force Microscopy. *J. Membr. Sci.* **2012**, *396*, 38−42.
(17) Park, J. Y.; Park, S.; Choe, W.; Yong, H. I.; Jo, C.; Kim, K. Plasma-Functionalized Solution: A Potent Antimicrobial Agent for Biomedical Applications from Antibacterial Therapeutics to Biomaterial Surface Engineering. *ACS Appl. Mater. Interfaces* **2017**, *9*, 43470−43477.
(18) Fisher, E. R. Challenges in the Characterization of Plasma-Processed Three-Dimensional Polymeric Scaffolds for Biomedical Applications. *ACS Appl. Mater. Interfaces* **2013**, *5*, 9312−9321.
(19) Wu, S.; Liu, X.; Yeung, A.; Yeung, K. W. K.; Kao, R. Y. T.; Wu, G.; Hu, T.; Xu, Z.; Chu, P. K. Plasma-Modified Biomaterials for Self-Antimicrobial Applications. *ACS Appl. Mater. Interfaces* **2011**, *3*, 2851−2860.
(20) Luan, P.; Knoll, A. J.; Bruggeman, P. J.; Oehrlein, G. S. Plasma−Surface Interaction at Atmospheric Pressure: A Case Study of Polystyrene Etching and Surface Modification by Ar/O2 Plasma Jet. *J. Vac. Sci. Technol., A* **2017**, *35*, No. 05C315.
(21) Luan, P.; Knoll, A. J.; Wang, H.; Kondeti, V. S. S. K.; Bruggeman, P. J.; Oehrlein, G. S. Model Polymer Etching and Surface Modification by a Time Modulated RF Plasma Jet: Role of Atomic Oxygen and Water Vapor. *J. Phys. D: Appl. Phys.* **2017**, *50*, No. 03LT02.
(22) Toros, A.; Kiss, M.; Graziosi, T.; Sattari, H.; Gallo, P.; Quack, N. Precision Micro-Mechanical Components in Single Crystal Diamond by Deep Reactive Ion Etching. *Microsyst. Nanoeng.* **2018**, *4*, 12.
(23) Girardot, C.; Böhme, S.; Archambault, S.; Salaün, M.; Latu-Romain, E.; Cunge, G.; Joubert, O.; Zelsmann, M. Pulsed Transfer Etching of PS−PDMS Block Copolymers Self-Assembled in 193 nm Lithography Stacks. *ACS Appl. Mater. Interfaces* **2014**, *6*, 16276−16282.
(24) Terashima, C.; Arihara, K.; Okazaki, S.; Shichi, T.; Tryk, D. A.; Shirafuji, T.; Saito, N.; Takai, O.; Fujishima, A. Fabrication of Vertically Aligned Diamond Whiskers from Highly Boron-Doped Diamond by Oxygen Plasma Etching. *ACS Appl. Mater. Interfaces* **2011**, *3*, 177−182.
(25) Smentkowski, V. S.; Moore, C. A. In-Situ Plasma Cleaning of Samples to Remove Hydrocarbon and/or Polydimethylsiloxane Prior to ToF-SIMS Analysis. *J. Vac. Sci. Technol., A* **2013**, *31*, No. 06F105.
(26) Bodas, D.; Khan-Malek, C. Hydrophilization and Hydrophobic Recovery of PDMS by Oxygen Plasma and Chemical Treatment—An SEM Investigation. *Sens. Actuators, B* **2007**, *123*, 368−373.
(27) Hillborg, H.; Gedde, U. W. Hydrophobicity Recovery of Polydimethylsiloxane after Exposure to Corona Discharges. *Polymer* **1998**, *39*, 1991−1998.
(28) Hillborg, H.; Ankner, J. F.; Gedde, U. W.; Smith, G. D.; Yasuda, H. K.; Wikström, K. Crosslinked Polydimethylsiloxane Exposed to Oxygen Plasma Studied by Neutron Reflectometry and Other Surface Specific Techniques. *Polymer* **2000**, *41*, 6851−6863.
(29) Lu, X.; Naidis, G. V.; Laroussi, M.; Reuter, S.; Graves, D. B.; Ostrikov, K. Reactive Species in Non-Equilibrium Atmospheric-Pressure Plasmas: Generation, Transport, and Biological Effects. *Phys. Rep.* **2016**, *630*, 1−84.
(30) Lu, X.; Laroussi, M. Optimization of Ultraviolet Emission and Chemical Species Generation from a Pulsed Dielectric Barrier Discharge at Atmospheric Pressure. *J. Appl. Phys.* **2005**, *98*, No. 023301.
(31) Mazur, T.; Grzybowski, B. A. Theoretical Basis for the Stabilization of Charges by Radicals on Electrified Polymers. *Chem. Sci.* **2017**, *8*, 2025−2032.
(32) Baytekin, H. T.; Baytekin, B.; Hermans, T. M.; Kowalczyk, B.; Grzybowski, B. A. Control of Surface Charges by Radicals as a Principle of Antistatic Polymers Protecting Electronic Circuitry. *Science* **2013**, *341*, 1368−1371.
(33) ASTM D5528 - 13 Standard Test Method for Mode I Interlaminar Fracture Toughness of Unidirectional Fiber-Reinforced Polymer Matrix Composites; https://www.astm.org/Standards/D5528.
(34) Baikie, I. D.; Venderbosch, E.; Meyer, J. A.; Estrup, P. J. Z. Analysis of Stray Capacitance in the Kelvin Method. *Rev. Sci. Instrum.* **1991**, *62*, 725−735.
(35) Ducati, T. R. D.; Simões, L. H.; Galembeck, F. Charge Partitioning at Gas−Solid Interfaces: Humidity Causes Electricity Buildup on Metals. *Langmuir* **2010**, *26*, 13763−13766.
(36) Sugimura, H.; Ishida, Y.; Hayashi, K.; Takai, O.; Nakagiri, N. Potential Shielding by the Surface Water Layer in Kelvin Probe Force Microscopy. *Appl. Phys. Lett.* **2002**, *80*, 1459−1461.
(37) Tanaka, M.; Imai, S.; Tanii, T.; Numao, Y.; Shimamoto, N.; Ohdomari, I.; Nishide, H. Nanometer-Sized Polyradical Particles: Organic Magnetic Dot Array Formed on a Silicon Microfabricated Substrate. *J. Polym. Sci., Part A: Polym. Chem.* **2007**, *45*, 521−530.
(38) Tanaka, M.; Saito, Y.; Nishide, H. Magnetic Force Microscopy as a New Tool to Evaluate Local Magnetization of Organic Radical Polymers. *Chem. Lett.* **2006**, *35*, 1414−1415.
(39) Angeloni, L.; Passeri, D.; Reggente, M.; Mantovani, D.; Rossi, M. Removal of Electrostatic Artifacts in Magnetic Force Microscopy by Controlled Magnetization of the Tip: Application to Superparamagnetic Nanoparticles. *Sci. Rep.* **2016**, *6*, 26293.
(40) Sugiyama, I.; Shibata, N.; Wang, Z.; Kobayashi, S.; Yamamoto, T.; Ikuhara, Y. Ferromagnetic Dislocations in Antiferromagnetic NiO. *Nat. Nanotechnol.* **2013**, *8*, 266−270.

DOI: 10.1021/acsapm.9b00532
ACS Appl. Polym. Mater. 2019, 1, 2638−2648

(41) Chen, D.-R.; Pui, D. Y. H. A High Efficiency, High Throughput Unipolar Aerosol Charger for Nanoparticles. *J. Nanopart. Res.* **1999**, *1*, 115−126.
(42) Dill, K. A.; Bromberg, S. *Molecular Driving Forces: Statistical Thermodynamics in Biology, Chemistry, Physics, and Nanoscience*, 2nd ed.; Garland Science: London, 2011.
(43) Fridman, A. A. *Plasma Chemistry*, 1st ed.; Cambridge University Press: Cambridge, 2008.
(44) Yuk, H.; Zhang, T.; Lin, S.; Parada, G. A.; Zhao, X. Tough Bonding of Hydrogels to Diverse Non-Porous Surfaces. *Nat. Mater.* **2016**, *15*, 190−196.
(45) Shaw, D.; West, A.; Bredin, J.; Wagenaars, E. Mechanisms behind Surface Modification of Polypropylene Film Using an Atmospheric-Pressure Plasma Jet. *Plasma Sources Sci. Technol.* **2016**, *25*, No. 065018.
(46) *Dusty Plasmas: Physics, Chemistry, and Technological Impacts in Plasma Processing*; Bouchoule, A., Ed.; Wiley: Chichester, 1999.
(47) Atala, E.; Velásquez, G.; Vergara, C.; Mardones, C.; Reyes, J.; Tapia, R. A.; Quina, F.; Mendes, M. A.; Speisky, H.; Lissi, E.; Ureta-Zañartu, M. S.; Aspée, A.; López-Alarcón, C. Mechanism of Pyrogallol Red Oxidation Induced by Free Radicals and Reactive Oxidant Species. A Kinetic and Spectroelectrochemistry Study. *J. Phys. Chem. B* **2013**, *117*, 4870−4879.

DOI: 10.1021/acsapm.9b00532
ACS Appl. Polym. Mater. 2019, 1, 2638−2648